Desalination and Water Treatment
www.deswater.com
doi: 10.5004/dwt.2019.24410

172 (2019) 359–367
December

Polyoxometalate composite electrode prepared through layer-by-layer assembly for efficient phenanthrene photoelectrodegradation

Qingfei Duan, Jianbo Guo*, Jingfang Lu*, Yuanyuan Song, Caicai Lu, Yi Han, Haibo Li

Tianjin Key Laboratory of Aquatic Science and Technology, School of Environmental and Municipal Engineering, Tianjin Chengjian University, Jinjing Road 26#, Tianjin 300384, China, Tel. +86 22 23085116; email: jianbguo@163.com (J. Guo), Tel. +86 22 23085117; emails: Lujfzz@126.com (J. Lu), Duanqf0426@163.com (Q. Duan), Song23735735@126.com (Y. Song), lucaicai2010@163.com (C. Lu), hanyi1127@126.com (Y. Han), lhb1980725@163.com (H. Li)

Received 3 January 2019; Accepted 14 May 2019

ABSTRACT

Polycyclic aromatic hydrocarbons (PAHs) are persistent environmental pollutants and the development of systems that transform or eliminate PAHs would be of great interest for both the human health and environmental protection. In this study, photoelectrocatalytic composite electrodes were successfully prepared for phenanthrene (PHE) degradation under low current density conditions. The electrodes were made of titanium dioxide (TiO_2) and phosphomolybdic acid (PMo_{12}) assembled through layer-by-layer to yield PMo_{12}/CNTs/TiO_2/Ti composites. The as-obtained electrodes were characterized by scanning electron microscopy, X-ray diffraction, and Raman spectroscopy. Electrochemistry showed PMo_{12}/CNTs/TiO_2/Ti electrodes to possess high photoelectrochemical activities due to broadened absorption spectra and solar light utilization efficiencies. The photoelectrocatalytic degradation of PHE was evaluated at different light sources at current density of 50 μA cm^{-2}. Under sunlight, PHE at concentrations around 1.5 mg L^{-1} were completely degraded within 60 min. The constant of zero-order kinetics for PHE degradation was estimated to 0.0227 mg L^{-1} min^{-1}, and the reaction was identified as surface-controlled catalysis. A mechanism of charge separation was also proposed. Overall, these findings look promising for future catalysis associated with environmental remediation.

Keywords: Polyoxometalate; Photoelectrocatalyst; Phenanthrene

1. Introduction

Polycyclic aromatic hydrocarbons (PAHs) are classified as pollutants due to their mutagenic, teratogenic, and carcinogenic properties. They are usually discharged into the environment from coking industry, oil spills, and waste oil processing [1–3]. PAHs are not only harmful to human health but also considered as ecological poison [1–4]. A total of 16 PAHs have been so far listed as priority pollutants by the United States Environmental Protection Agency (USEPA) [5], and more than 200 categories of PAHs have been observed of which most have carcinogenic properties. Hence, their transformation or elimination is urgent for human and environmental protection.

The remediation of PAHs contaminants is challenging because of their low water solubility, easy accumulation, and refractory. Despite this, many biological, physical, and chemical technologies exist for remediation of PAHs contamination. Among engineering processes, advanced oxidation processes (AOPs) are generally considered the best engineering routes due to their high rates and efficient transformations of organic pollutants. Recently clean energy-saving AOPs have attracted increasing attention, in which photoelectrocatalytic oxidation is an effective green

* Corresponding authors.

clean AOPs. Photoelectrocatalytic oxidation is defined as an electrochemically-assisted photocatalytic reaction technology [6]. Its quantum efficiency increases by reducing recombination of photogenerated electrons and holes through the application of an external bias to achieve complete mineralization of organic contaminants [7]. The activity of catalyst depends on the active components, which would determine the photoelectrocatalytic oxidation efficiencies. Hence, the selection of catalyst component is critical for successful remediation.

Titanium dioxides have been used as photocatalysts in many photoelectrocatalytic systems due to their high stabilities, elevated specific surface areas, relevant recyclability, and non-toxicity [8,9]. However, the high recombination of electrons and holes, as well as their large band-gap lead to low quantum efficiency. To improve quantum efficiency, previous studies focused on the preparation and modification of TiO_2 by nanocarbons as composite materials [10,11], yielding enhanced photocatalytic activities under visible light. Carbon acts as an electron trap to promote electron–hole separation, minimizing charge recombination and enhancing TiO_2 conductivity. However, most studies focused on nanoparticles which can hardly be recovered due to their easy aggregations after completion of the reaction. Hence, the preparation of composite films is more attractive since it prevents aggregation. A few studies dealing with the deposition of nanocarbon on TiO_2 nanotubes have so far been reported. The results overall showed good catalytic activities [10]. However, these traditional catalysts have low utilization of sunlight. Hence, novel TiO_2 based composites with superior catalytic activities and better stability are highly desirable.

Polyoxometalates have attracted increasing attention in photocatalysis thanks to their highest oxidation states with unmatched range of physical properties, such as electronic versatilities, redox characteristics, and unique molecular structures [12,13]. POMs as electron acceptors have also been applied to TiO_2 photocatalytic systems in an effort to enhance the conduction band and electron transfer rates for fast charge-pair recombinations [14,15]. Reduced POMs after accepting one or two conductive electrons on TiO_2 are relatively stable, and readily available for re-oxidization by transferring electrons to oxidants [16]. In this case, POMs act as electron transfer mediators between TiO_2 and electron acceptors. POMs could also absorb the ultraviolet light to produce photoelectrons. Hence, preparation of TiO_2, CNTs, and POMs composite electrodes are feasible routes for solving the catalytic problems.

Numerous potential techniques have so far been applied for modification of supports with POMs. These include electrodeposition [17], chemisorption [18], and layer-by-layer (LbL) self-assembly [19,20]. The LbL technique might yield polyelectrolyte multilayer films on substrates through alternate deposition of cationic and anionic aqueous solutions. This route can be used to introduce functional groups with controlled macroscopic properties or form interlayer structures for continuous reaction [21]. The LbL of POMs on substrates requires positively charged cationic linker molecules to anchor the negatively charged POMs anions. Polyelectrolytes are often used as linkers in most studies, including poly(allylamine hydrochloride) [20] and poly(diallyldimethylammonium chloride) [22]. On the other hand, room temperature ionic liquids (RTILs) consisting of ion pairs at or near room temperature have attracted increasing attention due to their excellent properties, such as non-volatility and enhanced electrochemical properties [23,24]. In addition, POMs-based hybrids have been synthesized from imidazole ionic liquids, and few applications in catalysis have been reported [19,22,23,25].

In this study, TiO_2 nanotube arrays were prepared by anodization, and CNTs were electrodeposited on TiO_2 nanotubes. Imidazolium-based cations derived from RTILs were employed as linkers for LbL modification of substrates with Keggin type POM molecules. Scanning electron microscopy (SEM), X-ray diffraction (XRD), and Raman spectroscopy were employed for characterization of the modified electrodes. The photoelectrochemical performances were evaluated through the degradation of phenanthrene (PHE) as target pollutant. The novel composite electrodes showed overall high photoelectrocatalytic abilities.

2. Experimental setup

2.1. Reagents

Phosphomolybdic acid (PMo_{12}) was purchased from Shanghai Titan Technology, Shanghai, China. Ti foil was obtained from Qinghe Jiarun Metallic Material, and CNTs from Nanjing XFNANO Material Technology. All other chemical reagents were of analytical grade unless otherwise specified and supplied by Tianjin Beichen Fangzheng Chemical Reagent Factory. The deionized water was prepared by our laboratory system.

2.2. Preparation of substrate CNTs/TiO_2/Ti

The electrode substrate was prepared using TiO_2/Ti and CNTs, starting by anodization of Ti followed by preparation of CNTs oxide and CNTs oxide electrodeposition.

2.2.1. Preparation TiO_2/Ti

Self-organized TiO_2 nanotube arrays were prepared by anodization of Ti foils (0.5 mm in thickness) in a bath containing ethylene glycol ($(CH_2OH)_2$), ammonium fluoride (NH_4F), and deionized water [26]. Before anodization, Ti foils were polished with 500 mesh sandpaper then ultrasonically cleaned in acetone, ethanol, and isopropanol. Anodization was carried out in an electrolyte containing 0.15 M NH_4F and 4% vol deionized water in $(CH_2OH)_2$ solvent. The cell was polarized at 50 V for 2 h using a DC power supply in a two-electrode system composed of a platinum cathode and Ti anode. Next, the anodized Ti foils were cleaned by deionized water and calcined at 450°C for 3 h. After cooling down to room temperature, the photoactive anatase phase (TiO_2/Ti) was employed as substrate for the electrodeposition of carbon nanotubes.

2.2.2. Preparation of CNTs oxide

The received CNTs were first purified before oxidation to remove any remaining metals and other amorphous carbon. They were then ultrasonically washed with concentrated

hydrochloric acid (HCl) for 45 min followed by washing with deionized water and drying. The resulting material was labeled as pCNTs. For functionalization, the pCNTs were further oxidized by wet chemical treatment [27]. To this end, pCNTs were first added to a solution containing sulfuric acid (H_2SO_4) and nitric acid (HNO_3) at a ratio of 3:1. The mixture was heated by reflux to 70°C for 8 h under constant stirring, followed by washing with deionized water and drying to yield functional CNTs (O-CNTs).

2.2.3. Electrodeposition

O-CNTs were deposited on TiO_2/Ti by electrodeposition [28]. The obtained O-CNTs were first ultrasonically dispersed in 0.1 M phosphate buffer solution (PBS, Na_2HPO_4 [pH = 9.18]) to form a black suspension with concentration of 0.5 mg mL^{-1}. Cyclic voltammetry was then applied to the black suspension in a three-electrode system connected to a CHI 660E electrochemical workstation. The calcined TiO_2/Ti was used as working electrode, platinum wire as counter, and saturated calomel as reference electrode. The scanning was performed from –1.5 to 0.5 V at 50 mV s^{-1} for 20 cycles. After deposition, the working electrode was washed with deionized water and dried at room temperature.

2.3. LbL process

For integrating the negatively charged POM catalysts by LbL assembly technique, 1-butyl-3-methylimidazolium hydrogen sulfate was used as a linker for modification of the substrate. In LbL coating, POMs were first dissolved in deionized water to form 5 mM coating solution. 1-Butyl-3-methylimidazolium hydrogen sulfate was then dissolved in deionized water to form 5 wt.% cation linker coating solution. The LbL process used to fabricate the composite electrode was performed according to several steps. First, the substrate was soaked in 9 M HNO_3 (2 min) then washed with deionized water (2 min). Next, the electrode was transferred into 5 wt.% ionic liquid solution (20 min) then washed with deionized water (2 min). Finally, it was soaked in 5 mM POM solution (20 min) followed by washing with deionized water (2 min).

2.4. Characterization

The surface morphologies of obtained electrodes were characterized by SEM (Hitachi S-4800). XRD (D/max-2500) with Cu Kα radiation was used for structure identification. Raman spectroscopy (D-35578 Wetzlar, Germany) was utilized for molecular structure determination. The electrochemical properties were evaluated on a CHI 600E workstation. All electrochemical experiments were performed in a three-electrode system containing Na_2SO_4 (0.01 mol L^{-1}) as electrolyte.

2.5. Phenanthrene degradation

The photoelectrocatalytic oxidation experiments were performed in an electrochemical cell under constant stirring to reduce mass transfer resistance. The three-electrode system was composed of composite electrode as working electrode, platinum foil as counter electrode, and saturated calomel electrode as reference electrode. Double display potentiometry was utilized for the oxidation process and performed for duration of 1 h. Phenanthrene was dissolved in methanol at concentration of 100 mg L^{-1} as mother liquid. Oxidation experiment electrolyte was prepared by the mother liquid and Na_2SO_4, and then 2.0 mL sample was taken and stored in refrigerator prior to detection. The phenanthrene concentration was determined by high-performance liquid chromatography (HPLC, Agilent 1100) equipped with UV detector and C_{18} reverse-phase column (inertsil ODS). The mobile phase contained a mixture of 20% deionized water and 80% methanol at total flow rate of 1.0 mL min^{-1}. The injection volume was 20 μL, and wavelength of UV absorbance detector was fixed at 254 nm.

3. Results and discussion

3.1. Characterizations of PMo_{12}/CNTs/TiO_2/Ti composite electrode

3.1.1. Scanning electron microscopy

The anodization of Ti foil in ammonium fluoride solution led to deposition of amorphous TiO_2 nanotubes on the anodized surface. Therefore, thermal treatment played an important role in transforming the amorphous phase into

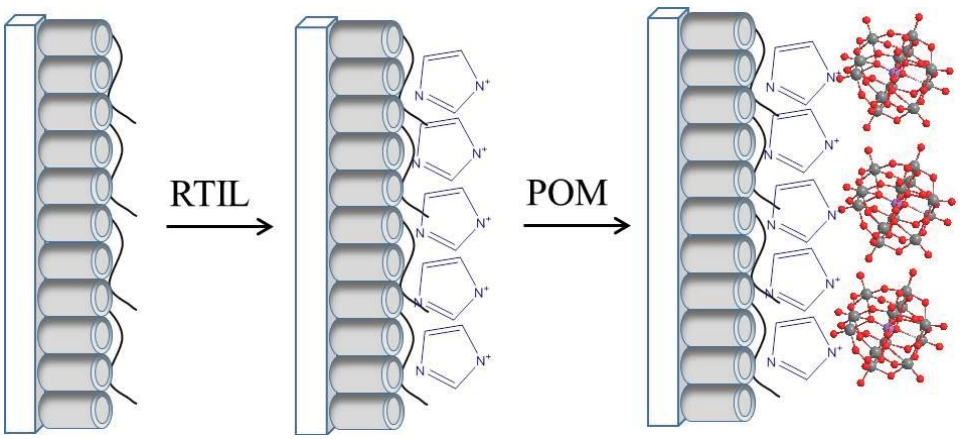

Fig. 1. Layer-by-layer self-assembly of composite electrode using POM and electrostatic linker, RTIL room temperature ionic liquids.

crystalline phase in muffle furnace. The SEM images of TiO_2 nanotube arrays are shown in Fig. 2a. The TiO_2 nanotubes looked to cover the entire Ti foil surface with high order and directional nanotube arrays with diameters of 60 nm. Fig. 2b depicts the SEM morphology of PMo_{12}/CNTs/TiO_2/Ti composite electrode. CNTs appeared well adhered to TiO_2 surface, meaning that CNTs were successfully electrodeposited on TiO_2 nanotubes at CNTs concentration of 0.5 mg mL^{-1} and deposition time of 1,600 s. On the other hand, POMs were not visible in SEM due to their small sizes and lack of agglomeration.

3.1.2. X-ray diffraction

XRD profiles of CNTs/TiO_2 and PMo_{12}/CNTs/TiO_2/Ti are shown in Fig. 3. The characteristic peaks at 2θ = 25.3°, 37.8°, 48.6°, and 55° were attributed to the (101), (004), (200), and (211) planes of anatase TiO_2 [10]. The main growth direction of TiO_2 was identified as (101) facets. The characteristic peaks at 2θ = 20°–30° were associated with carbon [29], indicating the electrodeposition of CNTs on TiO_2 nanotubes. The intensities of TiO_2 peaks decreased after combination with PMo_{12}. The characteristic peaks at 2θ = 22° and 28° were associated with Keggin structure with significant peak intensities, suggesting high dispersion of PMo_{12} on TiO_2 surface support without aggregation. These data were consistent with those from SEM.

3.1.3. Raman spectroscopy

The Raman spectrum of anatase phase showed characteristic peaks at 147, 197, 399, 515 (superimposed at 515 cm^{-1} bands), and 639 cm^{-1} [30]. These bands can be assigned to the six Raman active modes of anatase phase with symmetries of E_g, E_g, B_{1g}, A_{1g}, B_{1g}, and E_g, respectively. The major band of rutile phase appeared at 143 (superimposed at 143 cm^{-1} band due to rutile phase), 235, 447, 612, and 826 cm^{-1}. These bands were attributed to the B_{1g}, two-phonon scattering, E_g, A_{1g}, and B_{2g} modes, respectively. In Fig. 4, five peaks at 147, 199, 397, 513, and 636 cm^{-1} were visible. The strongest mode at 147 cm^{-1} (E_g) was 10-fold greater than any other phonon intensity arising from external vibration of anatase structure, suggesting formation of anatase phase with long-range order in annealed film. The bands at 1,346 and 1,602 cm^{-1} corresponded to *D* and *G* bands of MWCNTs [31]. The *G* band was assigned to E_{2C} first order mode issued from tangential oscillations of carbon atoms, indicative of high degree of crystallinity. The *D* band represented the double resonance caused by disordered graphite and defects in sp^2 skeleton. The I_D/I_G ratio is often used to quantify the degree of disorder in carbon frameworks. Here, it was estimated to 1.05, indicating relatively low degree of graphitization. This result was consistent with CNTs prepared by wet chemical oxidation by H_2SO_4/HNO_3. The Raman spectrum of PMo_{12} looked not that obvious since only small amounts of PMo_{12} were deposited on CNTs/TiO_2/Ti.

3.2. Electrochemistry

3.2.1. Photocurrent characteristics

A photocurrent response is often generated during separation of the photogenerated electron–hole pairs, and illumination increases the current that could result from photocarrier generation and carrier mobility enhancement. The responsiveness of PMo_{12}/CNTs/TiO_2/Ti composite electrode under interrupted light was studied at fixed bias voltage of 0 V vs. SCE. The potentiostatic plots of photocurrent

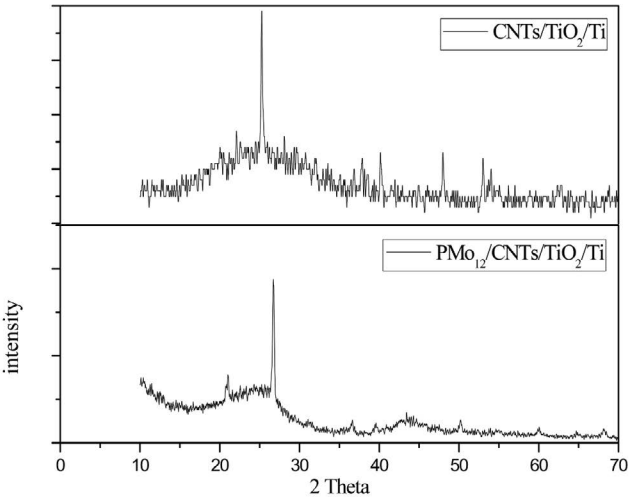

Fig. 3. XRD patterns of CNTs/TiO_2/Ti and PMo_{12}/CNTs/TiO_2/Ti.

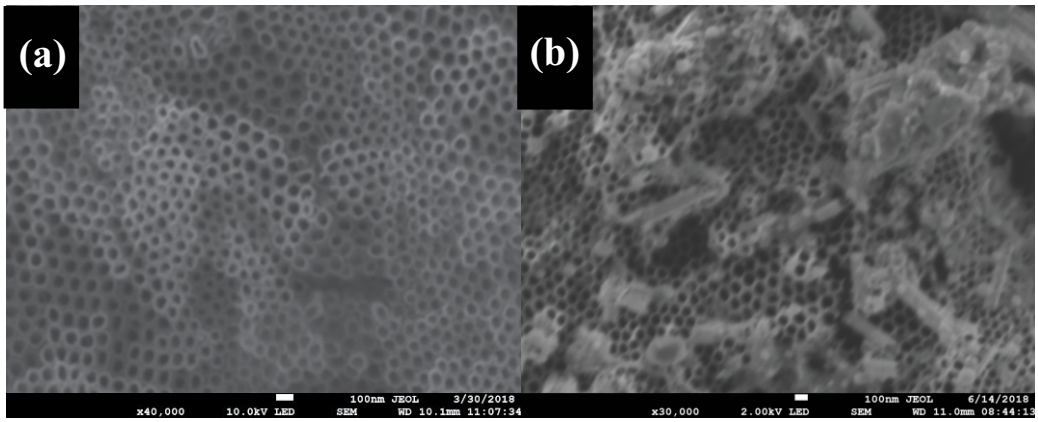

Fig. 2. SEM images of: (a) TiO_2 nanotubes and (b) composite electrode.

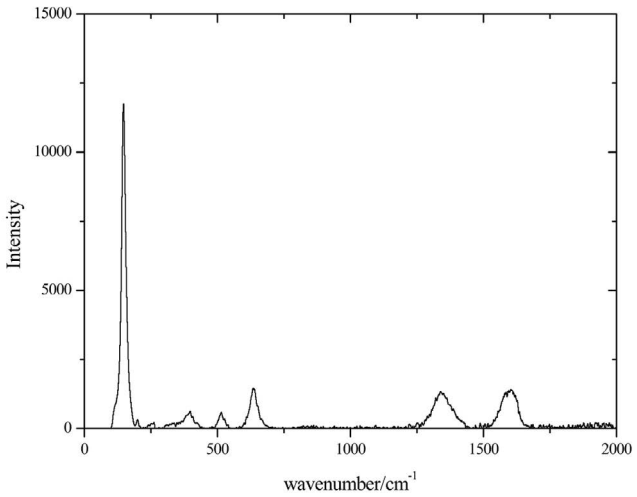

Fig. 4. Raman spectrum of composite electrode.

densities are displayed in Fig. 5. Promoted and stable photocurrent response was observed with the composite electrode and photocurrent reaching 1.25 mA. After photoreduction during the first "ON" light, the photocurrent response kept fairly stable under subsequent repetitive light irradiations, indicating robust adhesion between the film and underlying TiO_2. This would favor the direct use of the composite electrode as a whole.

3.2.2. Impedance properties

Electrochemical impedance spectroscopy (EIS) was used to examine the impedance properties of PMo_{12}/CNTs/TiO_2/Ti composite electrode and TiO_2/Ti electrode. Fig. 6 showed circular arcs with amplitudes decreased between TiO_2 and PMo_{12}/CNTs/TiO_2/Ti composite electrode. To better determine the roles of CNTs in PMo_{12}/CNTs/TiO_2/Ti composite electrode, the EIS of CNTs/TiO_2/Ti electrode was also measured. Obviously, CNTs/TiO_2/Ti electrode substrate and PMo_{12}/CNTs/TiO_2/Ti composite electrode depicted nearly identical circular arcs. The resistances of CNTs/TiO_2/Ti electrode substrate and PMo_{12}/CNTs/TiO_2/Ti composite electrode were much smaller than that of pure TiO_2 electrode. This suggested that CNTs promoted the electron transfer during the electrochemical reaction at PMo_{12}/CNTs/TiO_2/Ti composite electrode as an electron mediator with high conductivity.

3.3. Photoelectrocatalytic degradation of PHE

The efficiency of PMo_{12}/CNTs/TiO_2/Ti composite electrode toward PAHs degradation was studied using PHE as representative pollutant. Based on the conditions (with or without POM and light), three experiments were designed under the electrochemical system: visible light/ electrochemical, electrochemical system, and sunlight/electrochemical of PMo_{12}/CNTs/TiO_2/Ti electrode. For comparison, the ultraviolet light/electrochemical system using CNTs/TiO_2/Ti electrode substrate as working electrode was also studied (Figs. 7a and b). All systems were explored at 50 μA cm^{-2}. The degradation rate of PHE using CNTs/TiO_2/Ti reached 40% after 60 min reaction. In presence of PMo_{12}, the degradation rate of PHE was only 50%, meaning that PHE was hard to degrade at low current densities, consistent with previous other reports [32]. However, the result demonstrated that PMo_{12} acted as a catalyst. Compared with the electrochemical system, the degradation rate of PHE improved in photoelectrocatalytic system. When CNTs/TiO_2/Ti was used as working electrode under ultraviolet light/ electrochemical system, the degradation rate of PHE reached 60%, which was equivalent to 20% increase when compared with the electrochemical system. This indicated that the electrode worked as photocatalyst and produced hydroxyl radicals from reactive oxygen species through radical chain reaction. Also, 60% degradation rate was obtained in the visible light/electrochemical system using PMo_{12}/CNTs/TiO_2/Ti as working electrode. An increase of 10% in degradation rate meant that PMo_{12} contributed to catalysis but not obvious when compared with PMo_{12}/CNTs/

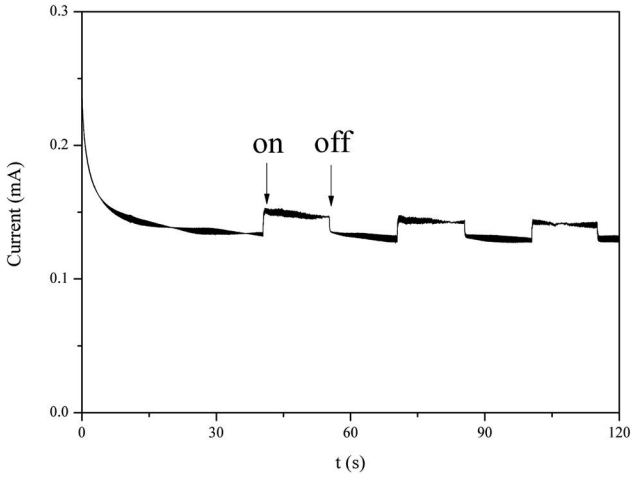

Fig. 5. Photocurrent characteristic of composite electrode.

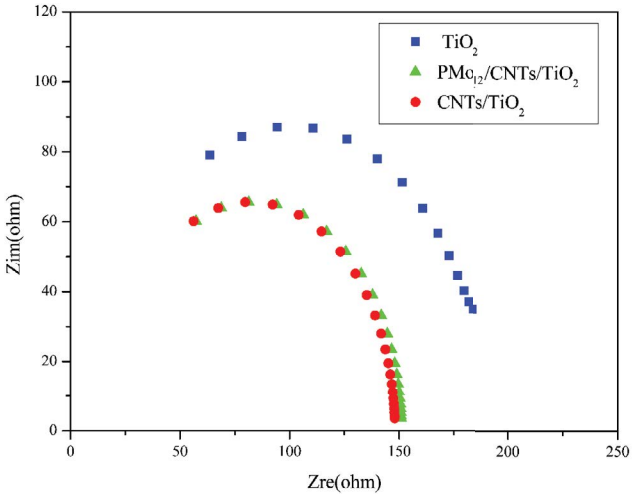

Fig. 6. EIS profiles of PMo_{12}/CNTs/TiO_2/Ti, TiO_2, and CNTs/TiO_2/Ti electrodes.

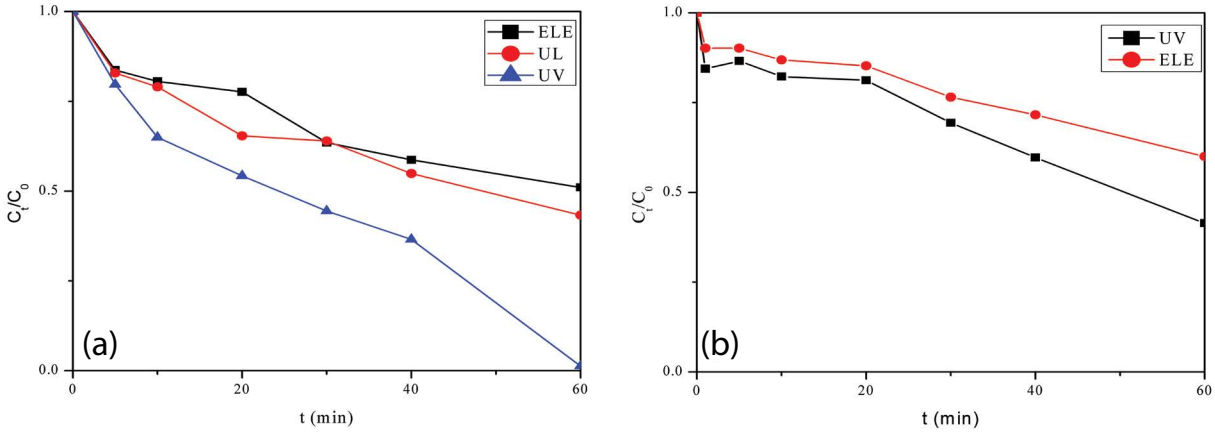

Fig. 7. PAHs degradation of PHE at concentration of 1.5 mg/L: (a) PMo_{12}/CNTs/TiO_2/Ti composite electrode and (b) CNTs/TiO_2/Ti substrate. ELE means electrocatalysis system, SL means sunlight photoelectrocatalysis system, and UL means visible light photoelectrocatalysis system.

TiO_2/Ti under the electrochemical system. This revealed that the composite electrode reduced the band-gap width of TiO_2. Finally, PHE was completely degraded after 60 min in sunlight/electrochemical system, which suggested the presence of synergetic catalytic effect between PMo_{12} and ultraviolet light in this photoelectrocatalytic system, causing the generation of more hydroxyl radicals when compared with the visible light system. The reason for this might have to do with the absorption peak of PMo_{12} located in the ultraviolet region, Hence, PMo_{12} can produce hydroxyl radical under ultraviolet light due to the presence of organic compounds in the solution [16]. Furthermore, during the first 20 min, the curve of CNTs/TiO_2/Ti catalytic system appeared flat. This was attributed to PHE, which was quickly adsorbed on the electrode but cannot rapidly degrade. In other words, the rate of hydroxyl radicals production was the limiting step during the beginning of the reaction but later PHE adsorption rate became the limiting step. Such phenomenon was not observed for PMo_{12}/CNTs/TiO_2/Ti composite electrode during photoelectrocatalytic reaction, suggesting that composite electrode can quickly generate hydroxyl radicals in the reaction system. In other words, the limiting step throughout the reaction was PHE adsorption rate. Thus, the composite electrode was an efficient composite material useful for HE oxygenolysis under low current densities and sunlight/electrochemical system.

3.4. Stability

The stability is an essential feature of any catalyst destined for industrial applications. Hence, recycling experiments were carried out and the results are shown in Fig. 8. The electrode was reused for five consecutive cycles without obvious loss in catalytic activity, demonstrating preservation of the structural integrity of the modified electrode during recycling catalytic processes.

3.5. Reaction kinetics

To gain a better understanding of PHE degradation in photoelectrocatalytic oxidation system, the reaction kinetics

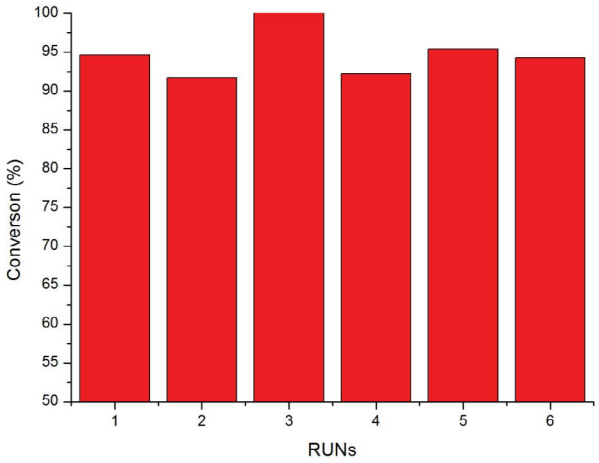

Fig. 8. Conversion yields for recycling experiments of catalyzed PHE.

was studied. The system was based on surface catalytic reactions, and degradation process of PHE followed zero-order kinetics. The zero-order rate constant of PHE degradation reaction was determined in ultrapure water without other reagents to ensure stable pH and initial concentration of PHE (1.5 mg L^{-1}). The kinetic equations are described in Eqs. (1) and (2).

$$-\frac{dC_{PHE}}{dt} = k \tag{1}$$

$$C_0 - C_{PHE} = kt \tag{2}$$

where C_{PHE} is concentration (mg L^{-1}) of PHE at reaction time t (min), C_0 is PHE concentration at time 0, and k is zero-order rate constant which could be calculated from the linear regression of ($C_0 - C_{PHE}$) as a function of time t.

The reaction constant was calculated as 0.0227 mg L^{-1} min^{-1} ($R^2 > 0.94$) after 60 min. Hence, the reaction was independent of reaction concentration and only linked to the surface

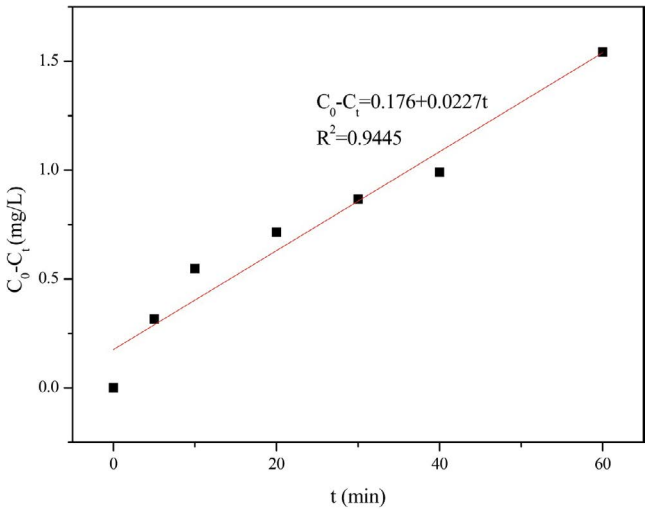

Fig. 9. Reaction kinetic curve of PHE at concentration of 1.5 mg L^{-1} in photoelectrocatalytic system under sunlight as light source.

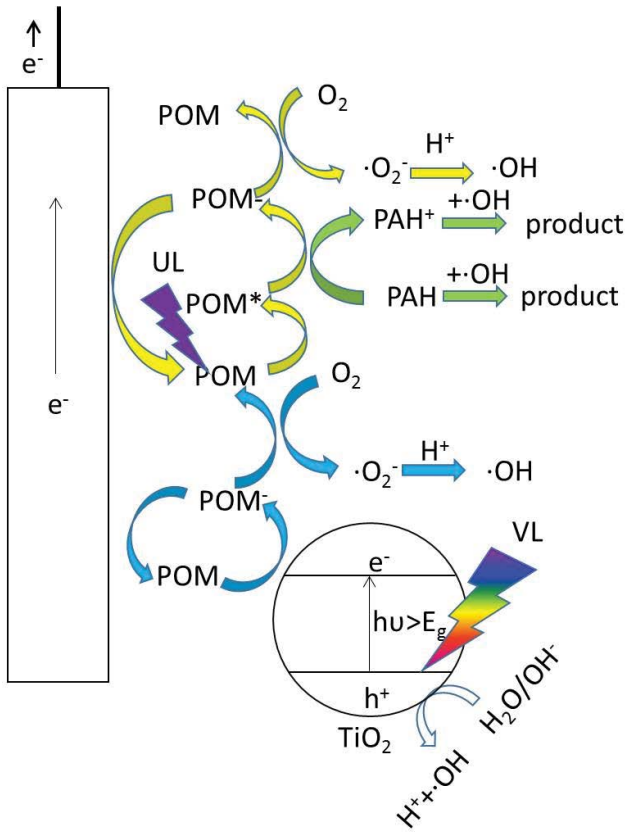

Fig. 10. Photoelectrocatalytic oxidation mechanism.

state. By considering the adsorption–desorption processes, the rate constant was calculated as 0.0208 mg L^{-1} min^{-1} after 40 min. Using substrate for PHE degradation, the reaction rate constant was estimated to 0.0183 mg L^{-1} min^{-1} (R^2 > 0.99) after 40 min. Under other conditions, the rate constants were recorded as: 0.0101 mg L^{-1} min^{-1} (R^2 > 0.96) (visible light/electrochemical), 0.01 mg L^{-1} min^{-1} (R^2 > 0.88) (electrocatalysis system), and 0.0154 mg L^{-1} min^{-1} (R^2 > 0.90) (sunlight photocatalysis system). Overall, the composite electrode showed a great photocatalytic activity toward the degradation of PHE.

3.6. Photoelectrocatalytic oxidation mechanism

AOPs are all chain-reaction sequences involving radical cycle propagation once radicals are formed [33]. In the proposed system, hydroxyl radicals were formed through two pathways. When visible light with photon energy (hν) was higher than band-gap energy of the semiconductor (E_g = 3.2 eV for anatase TiO_2), the valence band electrons of the semiconductor would undergo band-to-band transition. This will promote electrons from the valence band into the conduction band, inducing photogenerated electrons (e^-_{cb}) and holes (h^+_{vb}) according to Eq. (1) [34]. Part of the photogenerated holes (h^+_{vb}) would escape the direct recombination (Eq. (2)), and the other part of h^+_{vb} would reach TiO_2 surface with surface adsorbed hydroxyl groups or water to form adsorbed hydroxyl radicals ($^{\bullet}OH_{ads}$) according to Eqs. (3) and (4) [35]. The hydroxyl radical would then leave the surface toward bulk solution to form free hydroxyl radicals ($^{\bullet}OH_{free}$). Next, the photogenerated electron will migrate to POM through MWCNTs, leading to reduced-POM ($POM(e^-)_{red}$) (Eq. (5)) [36]. In other words, MWCNTs did not only act as electron transfer entities but also enhanced the efficiency of the electron use. Afterward, $POM(e^-)_{red}$ would be oxidized to POM with O_2 and transformed into $^{\bullet}O^-_{2ads}$ (Eq. (6)) [37]. Simultaneously, part of $POM(e^-)_{red}$ should become oxidized by the electrode reaction (Eq. (7)). O^-_{2ads} will generate hydroxyl radicals through free radical chain-reaction described by Eqs. (8)–(12) [7,14,35,38].

At ultraviolet light with hν higher than absorption threshold of POM, the POM will absorb light energy from the

Table 1
Proposed reaction mechanism

(1)	$TiO_2 + h\nu \rightarrow e^-_{cb} + h^+_{vb}$
(2)	$e^-_{cb} + h^+_{vb} \rightarrow$ heat
(3)	$h^+_{vb} + OH^-_{ads} \rightarrow {}^{\bullet}OH_{ads}$
(4)	$h^+_{vb} + H_2O \rightarrow H_2O^+ \rightarrow H^+ + {}^{\bullet}OH_{free}$
(5)	$e^-_{cb} + POM \rightarrow POM(e^-)_{red}$
(6)	$POM(e^-)_{red} + O_2 \rightarrow POM + {}^{\bullet}O^-_{2ads}$
(7)	$POM(e^-)_{red} - e^- \rightarrow POM$
(8)	$^{\bullet}O^-_{2ads} + H^+ \rightarrow HO^{\bullet}_2$
(9)	$2HO^{\bullet}_2 \rightarrow H_2O_{2ads} + O_2$
(10)	$H_2O_{2ads} + {}^{\bullet}O^-_{2ads} \rightarrow {}^{\bullet}OH_{ads} + OH^- + O_2$
(11)	$H_2O_{2ads} + {}^{\bullet}OH_{ads} \rightarrow H_2O + HO^{\bullet}_2$
(12)	$HO^{\bullet}_2 + {}^{\bullet}OH_{ads} \rightarrow H_2O + O_2$
(13)	$POM + h\nu \rightarrow POM^*$
(14)	$POM^* + PAH \rightarrow POM(e^-)_{red} + PAH^+$
(15)	$PAH(PAH^+) + {}^{\bullet}OH \rightarrow$ oxid. production

ground state to move to the excited state (POM*) (Eq. (13)) [16]. According to Eq. (14), POM* would obtain electron from PAH to yield reduced state ($POM(e^-)_{red}$) [16]. The rest of the process was consistent with the first pathway. In sum, POM, MWCNTs, and TiO_2-yielded heterogeneous composite catalyst with synergistic catalysis effect due to the different components. Finally, organic pollutants were oxidized to smaller molecule organic matter and inorganic matter, such as CO_2 and H_2O.

4. Conclusions

Novel PMo_{12}/CNTs/TiO_2/Ti composite electrode was prepared through LbL assembly. Compared with substrate CNTs/TiO_2/Ti, the PMo_{12}/CNTs/TiO_2/Ti composite electrode showed extended light absorption and facilitated separation/transfer of photogenerated electron–hole pairs. This led to complete photoelectrocatalytic degradation of PHE (1.5 mg L^{-1}) under low currents densities (50 μA cm^{-2}) in sunlight photoelectrocatalytic system. The reaction kinetics was evaluated and zero-order rate constants were calculated for substrate and composite electrode in the photocatalytic system. It was shown that the photoelectrocatalytic system was governed by surface catalytic reactions. In addition, the composite electrode was reused for five consecutive cycles without obvious loss in catalytic activity, showing good stability during cyclic experiments. Overall, PMo_{12}/CNT/TiO_2/Ti composite looks a promising candidate for disposal of PAHs from wastewaters.

Acknowledgments

This work was supported by the National Natural Science Foundation of China (Grant No. 51678387 and 51708389), Key project of Tianjin Education Commission Scientific Research Plan (Grant No. 2017KJ056), and Key project of Tianjin Natural Science Foundation (Grant No. 17JCZDJC39300).

References

[1] S. Yu, X. Gu, S. Lu, Y. Xue, X. Zhang, M. Xu, Z. Qiu, Q. Sui, Degradation of phenanthrene in aqueous solution by a persulfate/percarbonate system activated with CA chelated-Fe(II), Chem. Eng. J., 333 (2018) 122–131.

[2] R. Li, Y. Liu, W. Cheng, W. Zhang, G. Xue, S. Ognier, Study on remediation of phenanthrene contaminated soil by pulsed dielectric barrier discharge plasma: the role of active species, Chem. Eng. J., 296 (2016) 132–140.

[3] M.R. Cave, J. Wragg, D.J. Beriro, C. Vane, R. Thomas, M. Riding, C. Taylor, An overview of research and development themes in the measurement and occurrences of polyaromatic hydrocarbons in dusts and particulates, J. Hazard. Mater., 360 (2018) 373–390.

[4] A. Muratova, N. Pozdnyakova, O. Makarov, M. Baboshin, B. Baskunov, N. Myasoedova, L. Golovleva, O. Turkovskaya, Degradation of phenanthrene by the rhizobacterium *Ensifer meliloti*, Biodegradation, 25 (2014) 787–795.

[5] L.H. Keith, W.A. Telliard, Priority pollutants: I-a perspective view, Environ. Sci. Technol., 13 (1979) 416–423.

[6] A. García, C. Fernandez-Blanco, J.R. Herance, J. Albero, H. García, Graphenes as additives in photoelectrocatalysis, J. Mater. Chem. A, 5 (2017) 16522–16536.

[7] S. Garcia-Segura, E. Brillas, Applied photoelectrocatalysis on the degradation of organic pollutants in wastewaters, J. Photochem. Photobiol., C, 31 (2017) 1–35.

[8] M. Wongaree, S. Chiarakorn, S. Chuangchote, T. Sagawa, Photocatalytic performance of electrospun CNT/TiO_2 nanofibers in a simulated air purifier under visible light irradiation, Environ. Sci. Pollut. Res. Int., 23 (2016) 21395–21406.

[9] H. Park, Y. Park, W. Kim, W. Choi, Surface modification of TiO_2 photocatalyst for environmental applications, J. Photochem. Photobiol., C, 15 (2013) 1–20.

[10] I. Ali, K. Park, S.R. Kim, J.O. Kim, Electrochemical anodization of graphite oxide-TiO_2 nanotube composite for enhanced visible light photocatalytic activity, Environ. Sci. Pollut. Res. Int., 26 (2019) 1072–1081.

[11] H. Wu, J. Sun, D. Qi, C. Zhou, H. Yang, Photocatalytic removal of elemental mercury from flue gas using multi-walled carbon nanotubes impregnated with titanium dioxide, Fuel, 230 (2018) 218–225.

[12] Y.-F. Song, R. Tsunashima, Recent advances on polyoxometalate-based molecular and composite materials, Chem. Soc. Rev., 41 (2012) 7384–7402.

[13] I.V. Kozhevnikov, Catalysis by heteropoly acids and multicomponent polyoxometalates in liquid-phase reactions, Chem. Rev., 98 (1998) 171–198.

[14] G.R. Bertolini, L.R. Pizzio, A. Kubacka, M.J. Muñoz-Batista, M. Fernández-García, Composite $H_3PW_{12}O_{40}$–TiO_2 catalysts for toluene selective photo-oxidation, Appl. Catal., B, 225 (2018) 100–109.

[15] D.A. Friesen, J.V. Headley, C.H. Langford, The photooxidative degradation of *N*-methylpyrrolidinone in the presence of $Cs_3PW_{12}O_{40}$ and TiO_2 colloid photocatalysts, Environ. Sci. Technol., 33 (1999) 3193–3198.

[16] R.R. Ozer, J.L. Ferry, Kinetic probes of the mechanism of polyoxometalate-mediated photocatalytic oxidation of chlorinated organics, J. Phys. Chem. B, 104 (2000) 9444–9448.

[17] Z. Tang, S. Liu, E. Wang, S. Dong, E. Wang, Preparation, structures, and electrochemistry of a new polyoxometalate-based organic/inorganic film on carbon surfaces, Langmuir, 16 (2000) 5806–5813.

[18] H. Wang, N. Kawasaki, T. Yokoyama, H. Yoshikawa, K. Awaga, Molecular cluster batteries of nano-hybrid materials between Keggin POMs and SWNTs, Dalton Trans., 41 (2012) 9863–9866.

[19] M. Genovese, K. Lian, Ionic liquid-derived imidazolium cation linkers for the layer-by-layer assembly of polyoxometalate-MWCNT composite electrodes with high power capability, ACS Appl. Mater. Interfaces, 8 (2016) 19100–19109.

[20] D. Jeon, H. Kim, C. Lee, Y. Han, M. Gu, B.-S. Kim, J. Ryu, Layer-by-layer assembly of polyoxometalates for photoelectrochemical (PEC) water splitting: toward modular PEC devices, ACS Appl. Mater. Interfaces, 9 (2017) 40151–40161.

[21] Y. Al Thaher, S. Latanza, S. Perni, P. Prokopovich, Role of poly-beta-amino-esters hydrolysis and electrostatic attraction in gentamicin release from layer-by-layer coatings, J. Colloid Interface Sci., 526 (2018) 35–42.

[22] M. Genovese, Y.W. Foong, K. Lian, Designing polyoxometalate based layer-by-layer thin films on carbon nanomaterials for pseudocapacitive electrodes, J. Electrochem. Soc., 162 (2015) A5041–A5046.

[23] S. Herrmann, A. Seliverstov, C. Streb, Polyoxometalate-ionic liquids (POM-ILS)–the ultimate soft polyoxometalates? A critical perspective, J. Mol. Eng. Mater., 2 (2014) 1440001.

[24] A. Berthod, M.J. Ruiz-Ángel, S. Carda-Broch, Recent advances on ionic liquid uses in separation techniques, J. Chromatogr. A, 1559 (2018) 2–16.

[25] D.M. Fernandes, C.M.A. Brett, A.M.V. Cavaleiro, Layer-by-layer self-assembly and electrocatalytic properties of poly (ethylenimine)-silicotungstate multilayer composite films, J. Solid State Electrochem., 15 (2010) 811–819.

[26] C.W. Lai, S. Sreekantana, Higher water splitting hydrogen generation rate for single crystalline anatase phase of TiO_2 nanotube arrays, Eur. Phys. J. Appl. Phys., 59 (2012) 20403.

[27] K.A. Wepasnick, B.A. Smith, K.E. Schrote, H.K. Wilson, S.R. Diegelmann, D.H. Fairbrother, Surface and structural characterization of multi-walled carbon nanotubes following different oxidative treatments, Carbon, 49 (2011) 24–36.

[28] C. Liu, Y. Teng, R. Liu, S. Luo, Y. Tang, L. Chen, Q. Cai, Fabrication of graphene films on TiO_2 nanotube arrays for photocatalytic application, Carbon, 49 (2011) 5312–5320.
[29] X. Zhang, P. Lu, X. Cui, L. Chen, C. Zhang, M. Li, Y. Xu, J. Shi, Probing the electro-catalytic ORR activity of cobalt-incorporated nitrogen-doped CNTs, J. Catal., 344 (2016) 455–464.
[30] X. Wang, J. Shen, Q. Pan, Raman spectroscopy of sol–gel derived titanium oxide thin films, J. Raman Spectrosc., 42 (2011) 1578–1582.
[31] J. Luo, Y. Liu, H. Wei, B. Wang, K.-H. Wu, B. Zhang, D.S. Su, A green and economical vapor-assisted ozone treatment process for surface functionalization of carbon nanotubes, Green Chem., 19 (2017) 1052–1062.
[32] E. Mousset, N. Oturan, E.D. van Hullebusch, G. Guibaud, G. Esposito, M.A. Oturan, Treatment of synthetic soil washing solutions containing phenanthrene and cyclodextrin by electro-oxidation. Influence of anode materials on toxicity removal and biodegradability enhancement, Appl. Catal., B, 160–161 (2014) 666–675.
[33] J.L. Wang, L.J. Xu, Advanced oxidation processes for wastewater treatment: formation of hydroxyl radical and application, Crit. Rev. Env. Sci. Technol., 42 (2012) 251–325.
[34] A. Mills, S. Le Hunte, An overview of semiconductor photocatalysis, J. Photochem. Photobiol., A, 108 (1997) 1–25.
[35] Y. Chen, S. Yang, K. Wang, L. Lou, Role of primary active species and TiO_2 surface characteristic in UV-illuminated photodegradation of Acid Orange 7, J. Photochem. Photobiol., A, 172 (2005) 47–54.
[36] C. Gu, C. Shannon, Investigation of the photocatalytic activity of TiO_2–polyoxometalate systems for the oxidation of methanol, J. Mol. Catal. A: Chem., 262 (2007) 185–189.
[37] Q. Wang, E. Liu, C. Zhang, S. Huang, Y. Cong, Y. Zhang, Synthesis of $Cs_3PMo_{12}O_{40}/Bi_2O_3$ composite with highly enhanced photocatalytic activity under visible-light irradiation, J. Colloid Interface Sci., 516 (2018) 304–311.
[38] S. Zhu, D. Wang, Photocatalysis: basic principles, diverse forms of implementations and emerging scientific opportunities, Adv. Energy Mater., 7 (2017) 1700841.